Cork Open Research Archive
Cartlann Taighde Oscailte Chorcaí

Title	Charge compensation in trivalent cation doped bulk rutile TiO2
Author(s)	Iwaszuk, Anna; Nolan, Michael
Publication date	2011-08-02
Original citation	Iwaszuk, A. and Nolan, M. (2011) 'Charge compensation in trivalent cation doped bulk rutile TiO 2', Journal of Physics: Condensed Matter, 23(33), 334207 (11pp). doi: 10.1088/0953-8984/23/33/334207
Type of publication	Article (peer-reviewed)
Link to publisher's version	http://dx.doi.org/10.1088/0953-8984/23/33/334207 Access to the full text of the published version may require a subscription.
Rights	**© 2011 IOP Publishing Ltd. This is an author-created, un-copyedited version of an article accepted for publication in Journal of Physics: Condensed Matter. The publisher is not responsible for any errors or omissions in this version of the manuscript or any version derived from it. The Version of Record is available online at http://stacks.iop.org/0953-8984/23/i=33/a=334207**
Item downloaded from	http://hdl.handle.net/10468/5190

University College Cork, Ireland
Coláiste na hOllscoile Corcaigh

Charge Compensation in Trivalent Doped Bulk Rutile TiO$_2$

Anna Iwaszuk and Michael Nolan[*]

Tyndall National Institute, Lee Maltings, Cork, Ireland

* corresponding author. E-mail: michael.nolan@tyndall.ie

Abstract. Doping of TiO$_2$ is a very active field, with a particularly large effort expended using density functional theory (DFT) to model doped TiO$_2$; this interest has arisen from the potential of doping to be used in tuning the band gap of TiO$_2$ for photocatalytic applications. Doping is also of importance for modifying the reactivity of an oxide. Finally, dopants can also be unintentionally incorporated into an oxide during processing giving unexpected electronic properties. To unravel properly how doping impacts on the properties of a metal oxide requires a modelling approach that can describe such systems consistently. Unfortunately, DFT, as used in the majority of studies, is not suitable and in many cases cannot even give a qualitatively consistent description. In this paper we investigate doping of bulk rutile TiO$_2$ with trivalent cations, Al, Ga and In, using DFT, DFT corrected for on-site Coulomb interactions (DFT+U, with U on oxygen 2p states) and hybrid DFT (HSE06 functional) to better understand the performance of DFT in describing such fundamental doping scenarios and to analyse the charge compensation process with these dopants. With all dopants, DFT delocalises the oxygen hole polaron that results from substitution of Ti with the lower valent cation. DFT also finds an undistorted geometry and does not produce the characteristic polaron state in the band gap. DFT+U and hybrid DFT both localise the polaron, which is accompanied by a distortion to the structure around the oxygen hole site. DFT+U and HSE06 both give a polaron state in the band gap. The band gap underestimation present in DFT+U means that the offset of the gap state from both the valence and conduction band cannot be properly described, while the hybrid DFT offsets should be correct. We have investigated dopant charge compensation by formation of oxygen vacancies. Due to the large

number of calculations required, we use DFT+U for these studies. We find that the most stable oxygen vacancy site has either a very small positive formation energy or is negative, so that under typical experimental conditions, anion vacancy formation will compensate the dopant.

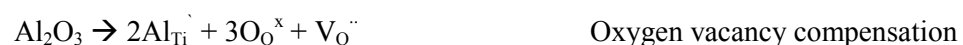PACS: 68.43.Bc, 68.55.Ln, 71.15.Mb, 73.20.Hb, 82.65.+r,

1. Introduction

Titanium dioxide is a technologically important material [1] continuing to gather considerable attention as a key material for clean energy production by photocatalytic water splitting [2-4]. Titania also has applications in coatings [5] and sensors [6] and is gaining more interest as a material for novel electronic memory devices, such as memristors [7].

In photocatalysis the relatively wide band gap of TiO_2, on the order of 3.1 eV, lies in the ultra violet and is too large for efficient use of solar energy, and there has been a tremendous amount of effort expended to examine experimental and modelling strategies for reducing the band gap towards the visible region [8 - 20]. The most widely used approach for what has been called "band gap engineering" has been to dope TiO_2 with another species, which could be a metal cation on the Ti site [8-13] or C/N/P on the anion site [14-17] or co-doping at cation and anion sites [18-20]. A single dopant introduces new states into the energy gap, in principle leading to a reduction of the band gap of the host oxide; whether this occurs at the valence band or at the conduction band depends on the dopant. It is assumed that these modifications of the electronic structure of the host oxide should lead to improved visible light absorption by pushing the band gap of TiO_2 towards the visible region of the electromagnetic spectrum. Improved photocatalytic efficiency will depend on how efficiently charge carriers can be separated and their lifetime, which cannot be estimated from the type of calculations carried out to date.

At the same time, many applications of TiO_2 require it *not* to be photocatalytically active [21-23], primarily in its role as a pigment in white paint; the photocatalytic activity of TiO_2 eventually leads to the "chalking" phenomenon, which is detrimental to the use of TiO_2 in pigments. In fact, it is worth recalling that the bulk of TiO_2 produced is used in applications where photocatalytic activity is not desired. To reduce the photocatalytic activity, some Al is added in small amounts to TiO_2 and can also be naturally present [21]. As a trivalent dopant, Al^{3+} has one less electron than Ti^{4+}, so that substituting one Ti^{4+} for Al^{3+} results in formation of an oxygen hole, i.e. an O^- polaron state, rather than the closed shell O^{2-} in the oxide. A second charge compensation mechanism can occur through oxygen vacancy formation, with one oxygen vacancy forming for two Al^{3+} dopants (similar to yttrium stabilised zirconia), giving the following defect reactions (in Kroger-Vink notation)

$$Al_2O_3 \rightarrow 2(Al'_{Ti} + O^{\cdot}_O) \qquad \text{Oxygen polaron}$$

$$Al_2O_3 \rightarrow 2Al_{Ti}^{'} + 3O_O^{x} + V_O^{\cdot\cdot} \qquad \text{Oxygen vacancy compensation}$$

Experiments have shown incorporation of Al onto Ti sites in TiO$_2$ [21, 22] and in particles, Al prefers to segregate to the surface. There have been some recent modelling studies of Al doped TiO$_2$, primarily using density functional theory [23-25]. As part of a study of defects in TiO$_2$, Islam *et al.* briefly noted that Al-doped into TiO$_2$ rutile with the hybrid PW1PW exchange-correlation functional (in the CRYSTAL code) results in formation of a localised oxygen hole [24]. Steshmans et al [25] showed with Hartree-Fock that Al-doping of TiO$_2$ produces an oxygen hole polaron. While HF does describe localised polarons, there are other issues with HF such as the overestimated band gap. Finally, Shirley *et al.* [23] used standard DFT to study Al doped anatase and rutile TiO$_2$, with no discussion of the electronic structure of the doped systems.

Other trivalent dopants have been less studied. This includes Ga^{3+}, which has been studied in a number of papers [26-29], and according to ref. 29, shows a small red shift in the band gap of TiO$_2$ after doping. Experimental results indicate that oxygen vacancies form to charge compensate the dopant [27]. Indium is another possible trivalent dopant for TiO$_2$ and in ref 30, Wang et al. claim that nanoparticles of TiO$_2$ doped with In show enhanced photocatalytic activity, consistent with earlier studies [31, 32].

For these dopants, there is a notable lack of first principles modelling studies to understand the fundamental microscopic aspects of these material systems. For TiO$_2$ in general, density functional theory (DFT) using approximate local exchange-correlation functionals is widely used, but this approach has some severe deficiencies. Two major problems with DFT are the band gap underestimation and the inability to properly describe localised defect states in oxides; refs 33-35 provide useful discussions of these issues. For the trivalent dopants, Al, Ga and In, Al doping, as noted above, has been treated with DFT [23] and hybrid DFT [24], without discussing the shortcomings of DFT for these systems and how to improve on the DFT description.

These issues with DFT are not solely confined to the question of doping in TiO$_2$, but are also of fundamental importance in the field of metal oxides. There are many other well known systems where the DFT description is entirely incorrect, such as reduced cerium dioxide [36 - 38], reduced vanadium pentoxide [39], and reduced TiO$_2$ [40 - 42]. These systems have reduced metal cations, which are localised on two metal centres, but for which DFT delocalises the electrons over all metal centres. Aliovalent doped oxides further highlight the inability of DFT to describe localised states; these include Li-doped MgO [43, 44] Al-doped SiO$_2$ [45, 46] and

La doped CeO_2 [47]. In these examples, the dopant has an oxidation state smaller than the cation it replaces so that oxygen ions near the dopant cannot achieve a closed shell O^{2-} configuration and instead an O^- species with a $2s^2 2p^5$ electronic configuration is formed; this oxygen shows features consistent with a polaron – a defect with a localised charge, coupled with a structural distortion.

Since the description of the example systems mentioned above is extremely challenging to DFT, we must go beyond this approach to even begin considering these systems. DFT corrected for on-site Coulomb interactions, DFT+U [48-50], in which a Hubbard U term is added to the DFT energy expression to describe localised electronic states, has been widely used to provide a reasonable and consistent description of the systems describe above [36-47]. However, there are many issues with DFT+U, not least of which is the empirical nature of the U parameter and the dependence of material properties on the value of U [51]. Finally, DFT+U persists in having an underestimation of the band gap, unless very large values of U are used [52], which in turn can deteriorate the other properties of the system. Despite this, DFT+U remains a useful, pragmatic approach to study problematic metal oxide systems, having the computational cost of a standard DFT calculation.

Hybrid DFT in a plane wave basis set has become the approach of choice for defects in metal oxides [53, 54] and has given for the first time a proper description of the band gap and the defect properties of oxides such as Cu_2O [55] and ZnO [56] and some multiferroic materials [57]. While hybrid DFT contains two parameters (exchange contribution and screening length), these are considered to be universal. With its recent successes, it is thus reasonable to assume that hybrid DFT will be useful for characterising doped metal oxides, and we have presented results of hybrid DFT calculations of ceria in refs. 58 and 59. However, hybrid DFT has an extremely large computational cost compared to standard DFT, *ca.* 50 times, which makes its application to large structures impossible and having extremely large time requirements even for systems of the size studied in this paper. We take a pragmatic approach, whereby we investigate the material with hybrid DFT and DFT+U, e.g. the formation of an oxygen hole polaron upon doping, and having established the consistency of the hybrid DFT and DFT+U approaches, we use DFT+U for subsequent calculations, such as charge compensating oxygen vacancies, where a large number of calculations are required.

Thus, this paper presents the results of a series of calculations of the trivalent metal dopants Al^{3+}, Ga^{3+} and In^{3+} in bulk rutile TiO_2. With a 3+ oxidation state, substituting a dopant onto a Ti^{4+} site, which is established

from experiments [21, 22, 27], will result in formation of an oxygen hole polaron and we demonstrate the inability of DFT to describe this defect, showing that DFT+U and hybrid DFT lead to polaron formation. The primary difference between DFT+U and hybrid DFT is in the position of the hole state in the TiO_2 band gap and we discuss this question. Finally, we investigate the energetics of oxygen vacancy compensation of the trivalent dopants.

2. Methodology

All calculations are carried out in the framework of periodic plane wave density functional theory (DFT) using the VASP code [60]. In this approach, the valence electronic states are expanded in a basis of periodic plane waves, with an energy cut-off of 400 eV, while the core-valence interaction is treated using PAW potentials [61], with an [Ar] core on Ti, [He] core on oxygen, [Ne] core on Al, [Ar] core on Ga and [Kr] core on In. The PW91 exchange-correlation functional [62] is used for DFT and DFT+U calculations; in the DFT+U calculations, U is applied to the O 2p states to describe the O$^-$ polaron and has a value of 7 eV [43, 45, 46, 47]; useful discussions of these polarons are given in refs [63 – 67]. For hybrid DFT, the screened exchange HSE06 functional [53, 54] is used, with the exchange contribution set at 25% and the screening parameter set to 0.2 / Å.

The bulk lattice parameter of rutile TiO_2 is relaxed with DFT and HSE, giving $a = b = 4.638$ Å and $c = 2.973$ Å (DFT) and $a = b = 4.593$ Å and $c = 2.948$ Å (HSE06), which are in reasonable agreement with experiment. A bulk (2 x 2 x 3) supercell expansion has been used in the DFT, DFT+U and hybrid DFT calculations. This cell expansion helps to reduce periodic defect-defect interactions. k-point sampling uses a (4 x 4 x 4) Monkhorst-Pack sampling grid for the bulk unit cell. The Methfessel-Paxton smearing scheme with a smearing parameter of 0.1 eV is used; this smearing parameter allows resolution of the peaks in the electronic density of states. All structures are fully relaxed until the forces are less than 0.02 eV/Å. No symmetry constraints are applied to the doped structures. For oxygen vacancy compensation we firstly added a second dopant to find the most stable dopant distribution. Next we remove one oxygen atom from several different sites in the structure with two dopants - as discussed in Sec. 3.3, 5 oxygen vacancy sites were considered - and calculate the formation energy from:

$$E^{vac} = E(M_xTi_{1-x}O_{2-y}) + 1/2E(O_2) - E(M_xTi_{1-x}O_2) \hspace{2cm} (1)$$

Where $E(M_xTi_{1-x}O_{2-y})$ is the total energy of two dopants in bulk TiO_2 with one oxygen vacancy, $E(M_xTi_{1-x}O_2)$ is the energy of two dopants in bulk TiO_2 and we reference to half the total energy of an O_2 molecule. A positive energy shows that there is a cost to form the oxygen vacancy. We use DFT+U to investigate dopant compensation, as the results below will show that it is a reliable approach when compared with hybrid DFT. As a further example of the reliability of the DFT+U results, we compute with DFT+U and Hybrid DFT the energy of incorporation of the dopant using the bulk metal as a reference. This energy is presented in table 1 and indicates that the trends in the energy of dopant incorporation is the same with both DFT approaches, with the larger ionic radius dopant requiring a higher energy for incorporation. The absolute values of the energies are also consistent between the two approaches.

Dopant	Al	Ga	In
	E^{doping} / eV	E^{doping} / eV	E^{doping} / eV
DFT+U	+1.46	+4.53	+5.57
Hybrid DFT	+2.37	+5.65	+6.81

Table 1: Energy to incorporate the trivalent dopants in bulk TiO_2 using the bulk metal as a reference, computed with DFT+U and Hybrid DFT.

3. Results

3.1 Atomic Structure of Doped Bulk Rutile TiO_2

Figure 1 shows the (2x2x3) bulk rutile unit cell, with the position of the dopant atom indicated by the blue sphere. Figure 2 (a) – (i) shows the local geometry around the dopant site for each dopant, from the three DFT approaches, while figure 3 shows the local geometry around the polaron site for each dopant, again with the three DFT approaches.
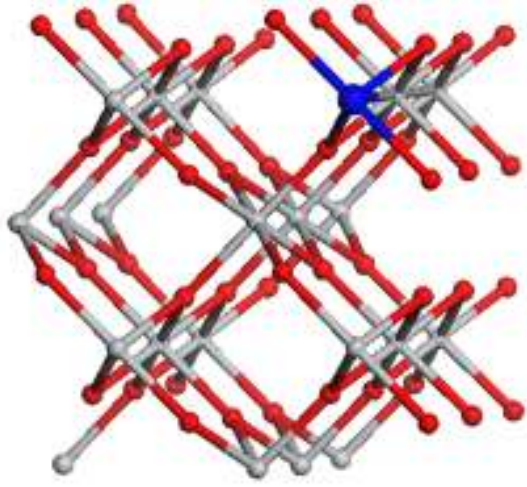
Figure 1: The bulk rutile (2 x 2 x 3) supercell. In this figure Ti is the grey sphere, oxygen is the red sphere and the dopant is generically indicated by a bulk sphere.

Firstly we point out that there are two general solutions for the structure and electronic structure of these doped systems. The first solution is symmetric, in which there is little distortion to the structure apart from changes in dopant-O distances due to the different sizes of the dopant and Ti. Therefore, the four equatorial dopant-O distances are equal and the two apical dopant-O distances are equal, but different to the equatorial dopant-O distances. The asymmetric solution has a geometrical distortion around the dopant so that the dopant-O distances are no longer the same.

We find with DFT that only the symmetric solution is stable, even when starting from a distorted solution, but with DFT+U and hybrid DFT, both symmetric and asymmetric solutions are stable. With DFT+U and hybrid DFT, the asymmetric solutions are the more stable, by *ca.* 0.4 eV and we will not discuss the symmetric solutions for these approaches any further.

The structural images in figure 2 show dopant-O distances in the immediate vicinity of the dopant from DFT, DFT+U and hybrid DFT for doping with Al (figure 2(a)-(c)), Ga (figure 2(d)-(f)) and In (figure 2(g)-(i)). In the DFT solution, figure 2(a), (d) and (g), the geometry around the dopant site is indeed symmetric. In bulk rutile the equatorial and apical Ti-O distances are 1.96 Å and 2.00 Å. The resulting dopant-O distances correlate with dopant ionic radius – the shortest dopant-O distances are found with Al^{3+} (the smallest ionic radius cation) and the longest distances with In^{3+} (the largest ionic radius cation) as dopant. Al^{3+} and Ga^{3+}

have been studied since it is thought that the similarity of their ionic radii to Ti^{4+} makes dopant incorporation favourable.

With DFT+U the symmetry around the dopant site appears to be broken for In but not, apparently, for Al^{3+} and Ga^{3+} doping, figure 2(b), (e) and (h). For Al^{3+} and Ga^{3+} doping, the pair of equatorial dopant-O distances and the four apical dopant-O distances show a small degree of symmetry breaking and are consistent with the dopant ionic radius. With In there the equatorial In-O distances are similar but the apical In-O distances show a distortion, with one In-O distance of 2.16 Å and the other being 2.08 Å.
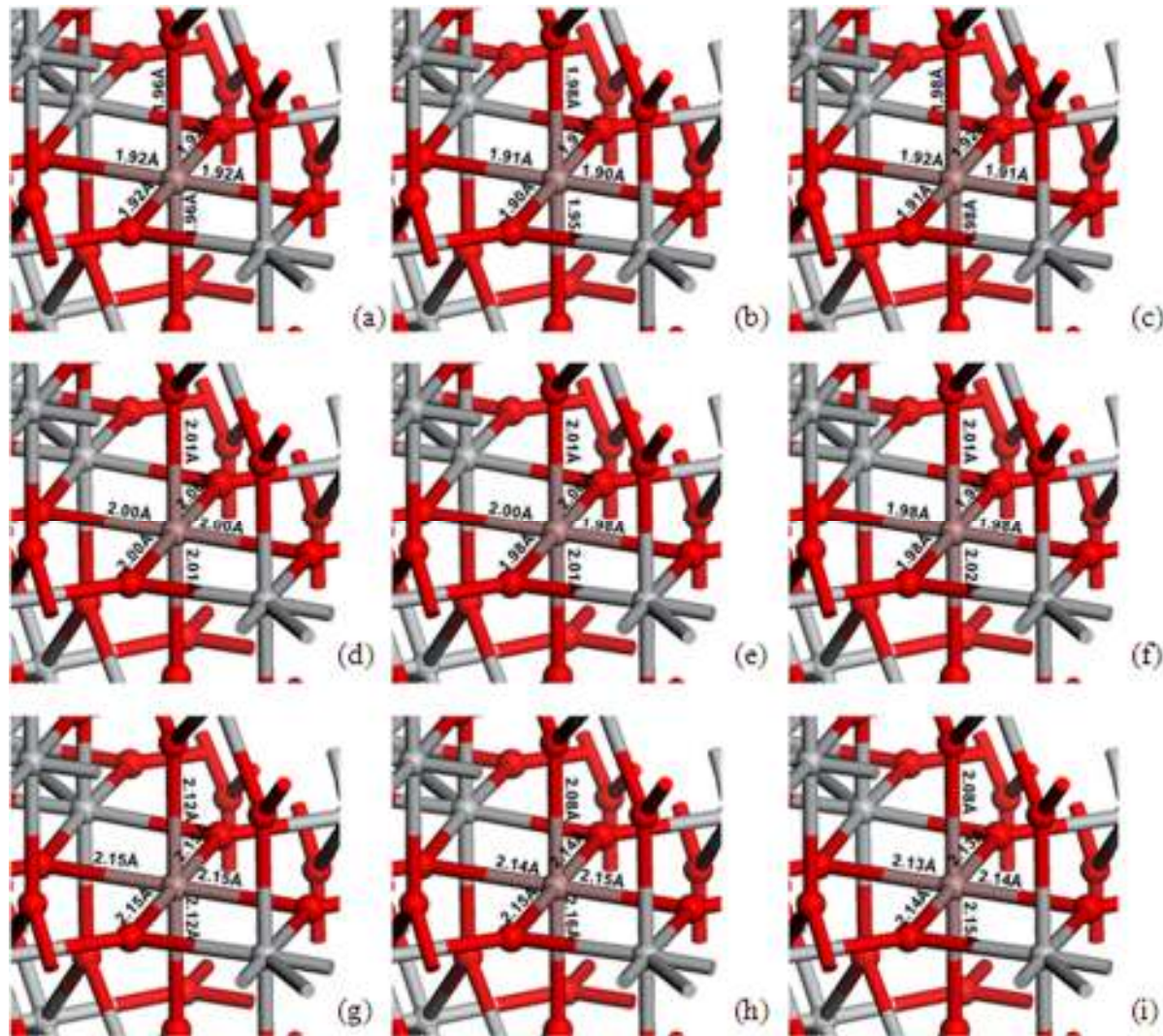
Figure 2: Structure around the dopant site for (a) Al DFT, (b) Al DFT+U, (c) Al HSE06, (d) Ga DFT, (e) Ga DFT+U, (f) Ga HSE06, (g) In DFT, (h) In DFT+U, (i) In HSE06

These results show that there are two types of distortion around the dopant, which can depend on the dopant ionic radius. The first is simply a distortion to the dopant-O distances compared to the Ti-O distances, due to the dopant ionic radius - in this case, the In dopant has the largest ionic radius and shows the longest cation-O distances. The second distortion is in the cation-O distances connected with the polaron. For In, the asymmetry in the apical In-O distances highlights this distortion, with one In-O distance appreciably lengthened, consistent with a longer bond between In and an oxygen polaron, as found in other materials [43-45,63-67]; we shall see in section 3.2 that electronic structure analysis confirms this picture. This particular distortion is not present for Al and Ga doping. With hybrid DFT, the distances are similar to DFT+U result, so that the same distortions around the dopants are present. This gives confidence in the DFT+U description of these systems.

If a polaron is present for Al and Ga, then it must be found on an oxygen not directly neighbouring the dopant site. We have examined the cation-O distances near the dopant site and figure 3 shows cation-O distances in the vicinity of the polaron site – the geometry is consistent with the presence of an oxygen polaron [43-47, 62-67]. For Al and Ga doping, the polaron is not directly bound to the dopant, but is instead in a next-nearest neighbour position, but for In, the dopant is directly bound to the polaron oxygen. Hence in figure 3, the Al and Ga sites are not shown, but the In site is shown.

Figure 3 shows for Al and Ga doping, the distortion of the cation-O distances around the polaron. For Al, there is one equatorial Ti-O distance of 2.15 Å (DFT+U) and 2.14 Å (HSE06), with a correspondingly shorter equatorial Ti-O distance of 1.85 Å (DFT+U) and 1.84 Å (HSE06) to another oxygen. With Ga, similar Ti-O distances are found and it is interesting to see that DFT+U and HSE predict the polaron site to be on different oxygen atoms. To examine the energetics of different solutions to the dopant-polaron distribution, we have used the DFT+U structure as input to a HSE06 calculation and *vice versa*. We have found that the hybrid DFT dopant-polaron distribution is essentially degenerate with the original DFT+U solution in DFT+U and the DFT+U dopant-polaron distribution is 22 meV higher in energy with hybrid DFT. Thus, similar to CeO_2 [37, 38] there are a number of stable polaron solutions that lie close in energy. Thus, an experimental investigation of such systems would observe an averaging over energetically accessible defect configurations, as has been discussed recently for TiO_2 [68].
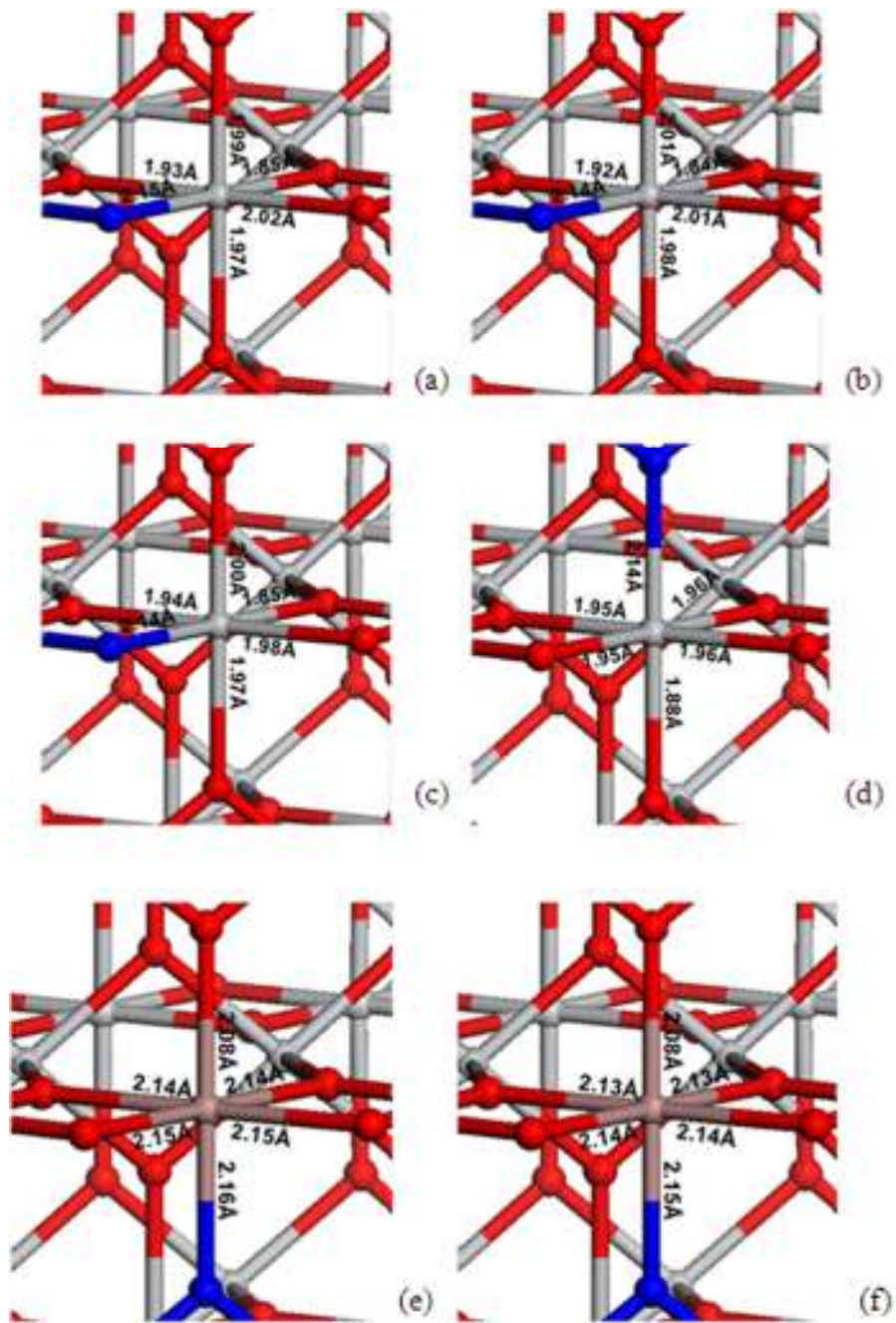
Figure 3. Structure around the polaron for (a) Al DFT+U, (b) Al HSE06, (c) Ga DFT+U, (d) Ga HSE06, (e) In DFT+U, (f) In HSE06. The blue sphere indicates the position of polaron. For Al and Ga, the polaron is not bound directly to the dopant, but for In the dopant and polaron are directly bound. Therefore, it is only for the case of In that the dopant is visible.

3.2 Electronic Structure of Doped TiO_2

To examine the destination of the oxygen hole (polaron) state resulting from doping with a trivalent dopant, figures 4 – 6 show the electronic density of states (EDOS) projected onto the O 2p states for Al doped TiO_2, Ga doped TiO_2 and In doped TiO_2, from the three DFT methods,. Also shown beside the EDOS plots is the excess spin density (defined as the difference between the spin up electron density and the spin down electron density). The spin density is used to show where the oxygen hole state is found in the structure.

For each dopant, DFT delocalises the oxygen hole over all oxygens in the structure for each dopant, while with DFT+U and HSE06, the hole is primarily localised on one oxygen ion near the dopant. This shows that the DFT+U approach, as used in this work, provides at least a consistent description of the formation of the polaron state in these doped systems, when compared to HSE06, which is known to provide a proper description of polaronic systems [54-56, 58].

The EDOS for the three doped systems are very similar. There is no state in the band gap with DFT, consistent with the delocalisation of the oxygen hole. Instead the hole state is found at the top of the VB, which is consistent with earlier findings for other oxides with these oxygen hole polarons [43, 45, 66, 67]. With DFT+U and hybrid DFT, a defect state is present in the TiO_2 band gap, which arises from the localised oxygen hole state shown in the spin density.
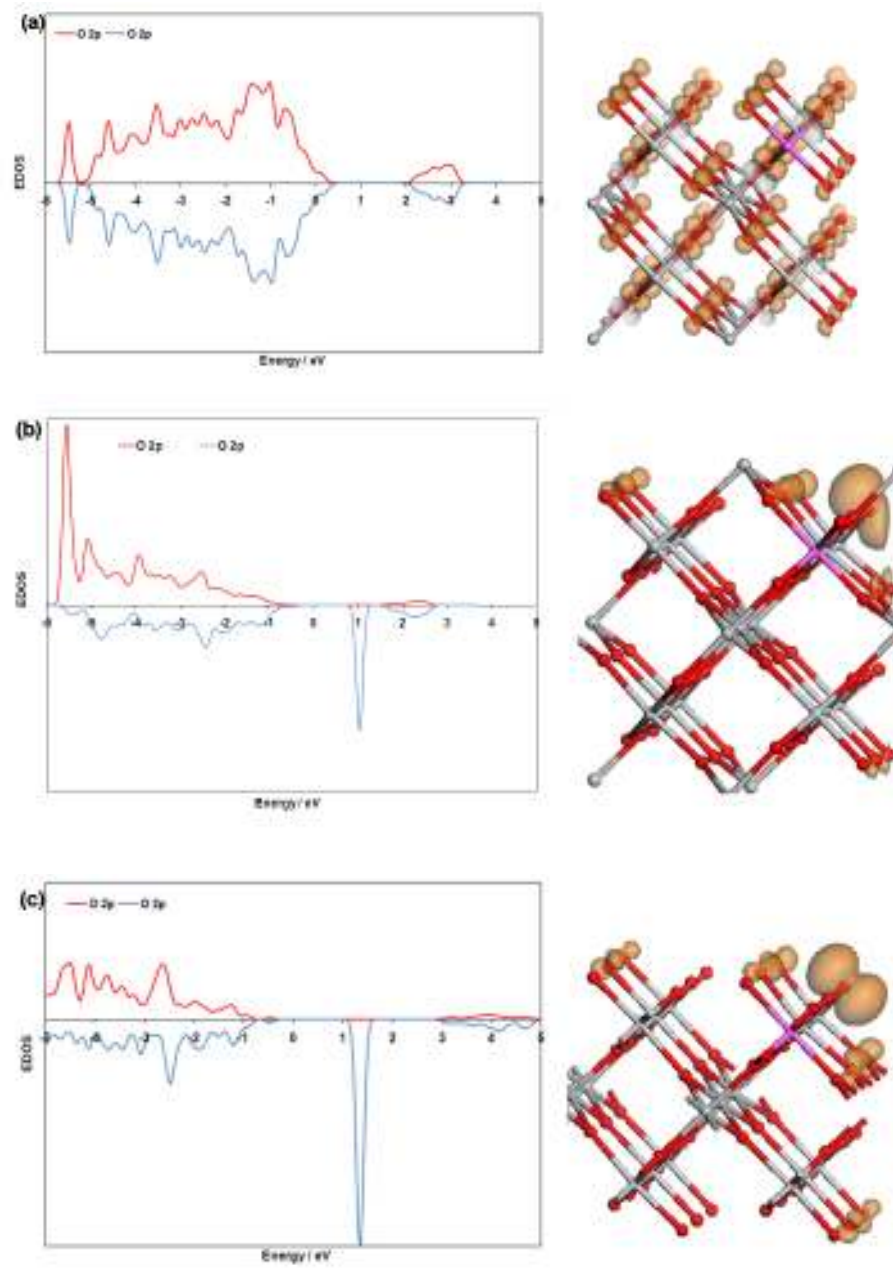
Figure 4: EDOS plots for Al doped bulk TiO_2. The right hand panel shows the spin density. (a) DFT, (b) DFT+U, (c) Hybrid DFT. The dopant is the purple sphere and the spin isosurfaces are set to 0.02 electrons / Å^3
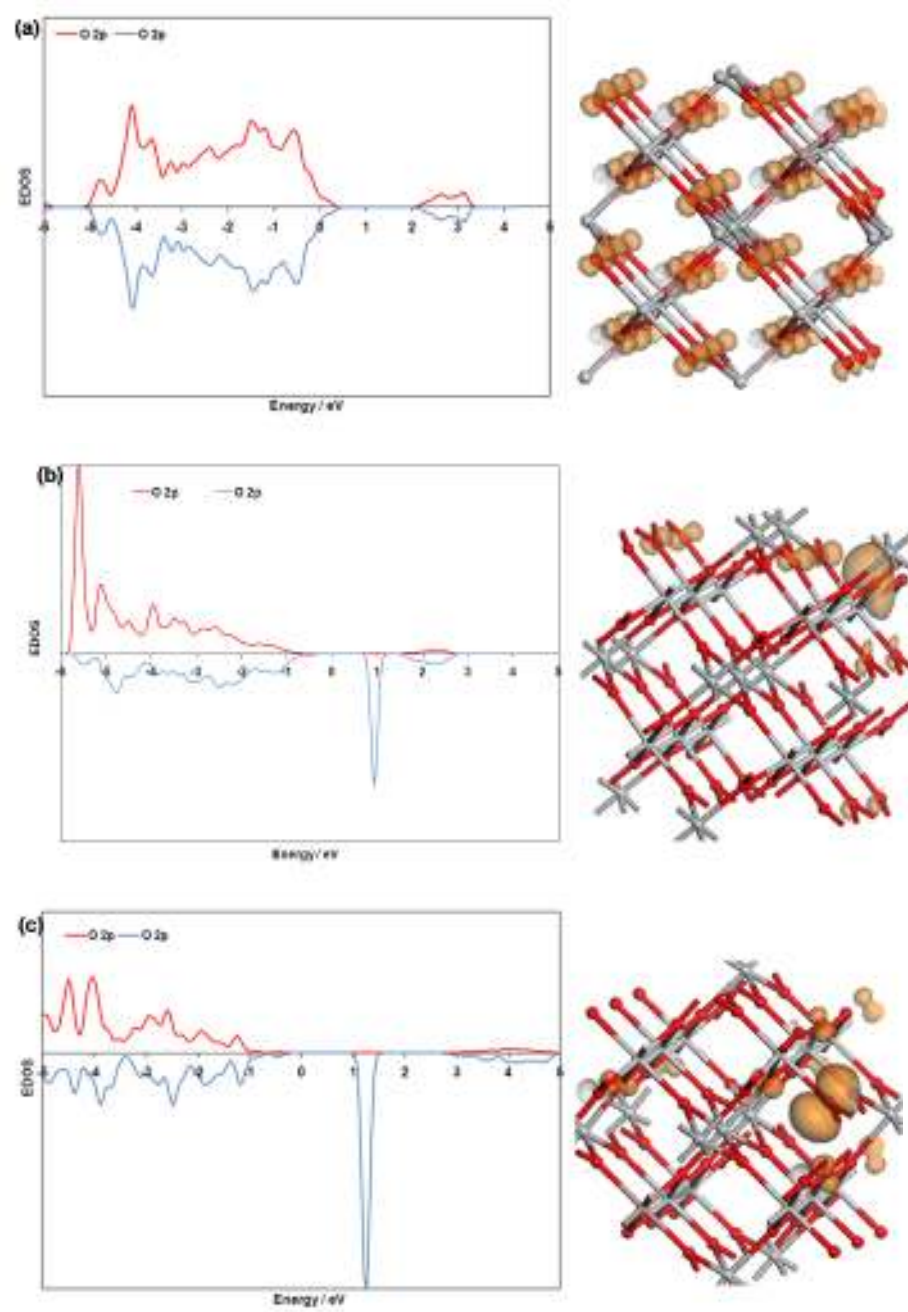
Figure 5: EDOS plots for Ga doped bulk TiO$_2$. The inset shows the spin density. (a) DFT, (b) DFT+U, (c) Hybrid DFT. The dopant is the purple sphere and the spin isosurfaces are set to 0.02 electrons / Å^3
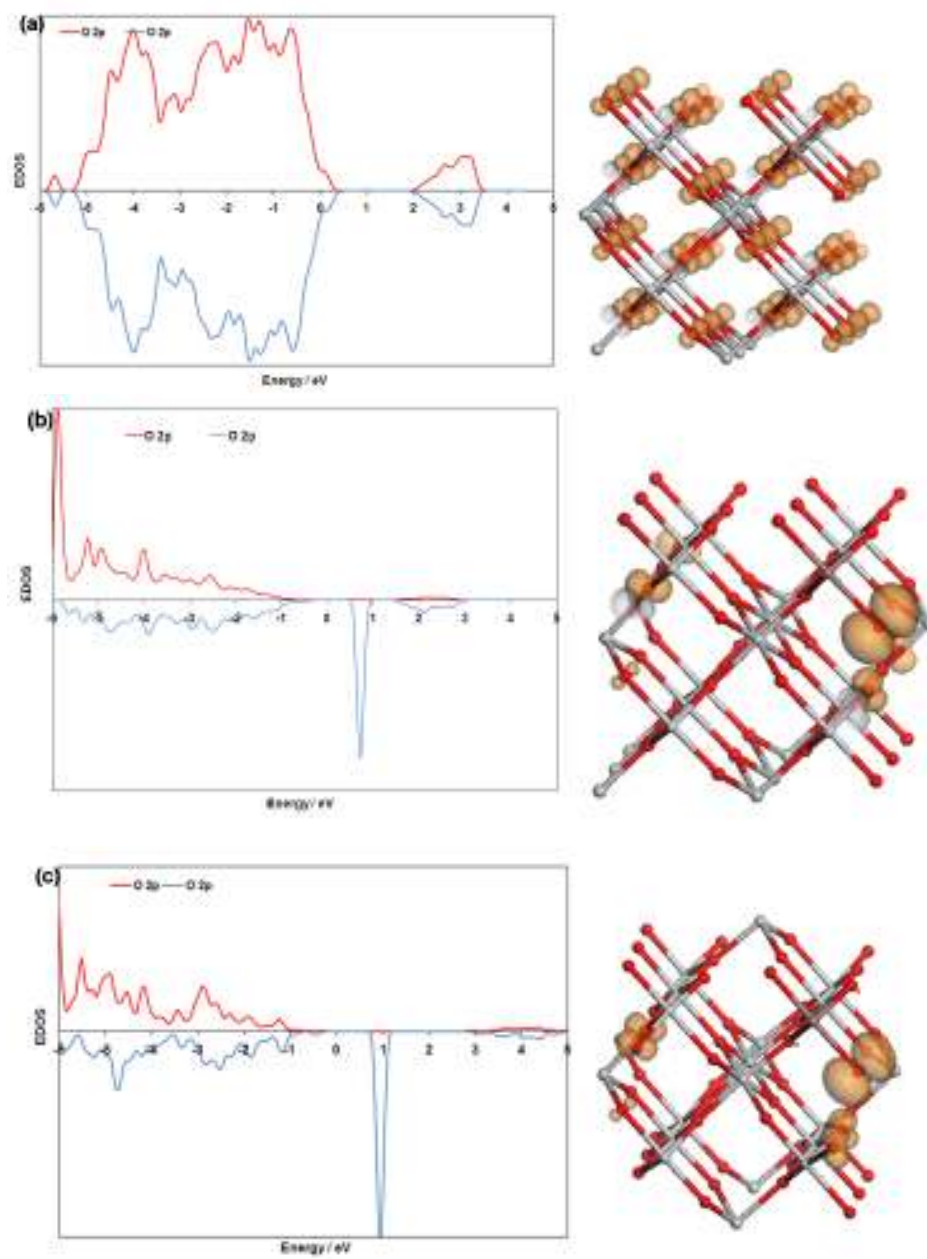
Figure 6: EDOS plots for In doped bulk TiO_2. The inset shows the spin density. (a) DFT, (b) DFT+U, (c) Hybrid DFT. The dopant is the brown sphere and the spin isosurfaces are set to 0.02 electrons / $Å^3$

However, the precise position of the defect state in the band gap is clearly dependent on the DFT approach used, with table 2 presenting the offsets of the polaron state from the valence and conduction band edges. Firstly, DFT+U predicts the offset of the polaron state from the valence band (VB) to within 0.35 eV of the hybrid DFT offset, with both methods placing the polaron state well inside the band gap of the oxide. But the

offset to the conduction band states is where there is a large difference: DFT+U predicts offsets no larger than 0.65 eV, while hybrid DFT predicts much larger offsets. The difference arises from the poor position of the conduction band states with DFT+U and the underestimated band gap, which are remedied by using hybrid DFT.

Dopant	Al		Ga		In	
	E^{VB} / eV	E^{CB} / eV	E^{VB} / eV	E^{CB} / eV	E^{VB} / eV	E^{CB} / eV
DFT+U	1.30	0.45	1.25	0.45	1.05	0.65
Hybrid DFT	1.65	1.55	1.55	1.65	1.25	1.95

Table 2: Offsets of the oxygen polaron defect state from the VB and CB for bulk TiO_2 doped with Al, Ga and In from DFT+U and Hybrid DFT. E^{VB} is the offset to the valence band and E^{CB} is the offset to the conduction band

The offset of the defect state to the VB should be well described with DFT+U since U is applied to the O 2p states and the defect state comes out of a previously O 2p-derived VB state. This value of U was determined by obtaining the position of the polaron state relative to the VB in Li-doped MgO [43], but can also be found from experimental data [69]. Since U has no effect on the conduction band states, which derive from Ti 3d orbtials, then DFT+U, as used here, cannot give the correct band gap and hence the correct offset of the defect state to the conduction band. One could envisage using a +U correction on Ti, but this would entail two +U corrections in one calculation, which has its own issues; see however ref. [70] where this approach was used successfully for defects in TiO_2. We expect that the hybrid DFT results will be correct and these results can provide a good check on the DFT+U findings.

Finally, if we consider the effect of U in the DFT+U calculation, then we have shown in ref. 45, that a smaller value of U on O 2p states moves the defect state away from the CB, but correspondingly reduces the offset to the VB edge, and leads to icnreased delocalisation of the oxygen hole. A larger value of U on O2p states would move the defect state closer the CB, so that we can highlight a key issue with DFT+U, namely that since the correct band gap cannot be obtained, then the position of defect states relative to the valence and

conduction bands cannot be obtained. Despite this, DFT+U provides a useful approach for doped systems such as considered herein.

3.3 Oxygen Vacancy Compensation

To study charge compensation of the dopant oxidation state by oxygen vacancy formation, we consider the defect formed by two dopants and an oxygen vacancy. In figure 7 we show four structures for dopant pairs with different dopant-dopant distances. We find that upon relaxation, the highest energy dopant distribution, relative to the most stable dopant pair structure, is less stable by only 0.5 eV. This small energy difference indicates that in a real system, there will be a distribution of these dopant pair configurations. Thus, for Al and In we show results for the most stable configuration and for Ga we present results for two dopant pair configurations. Thus our results can be considered representative for a typical dopant pair configuration.
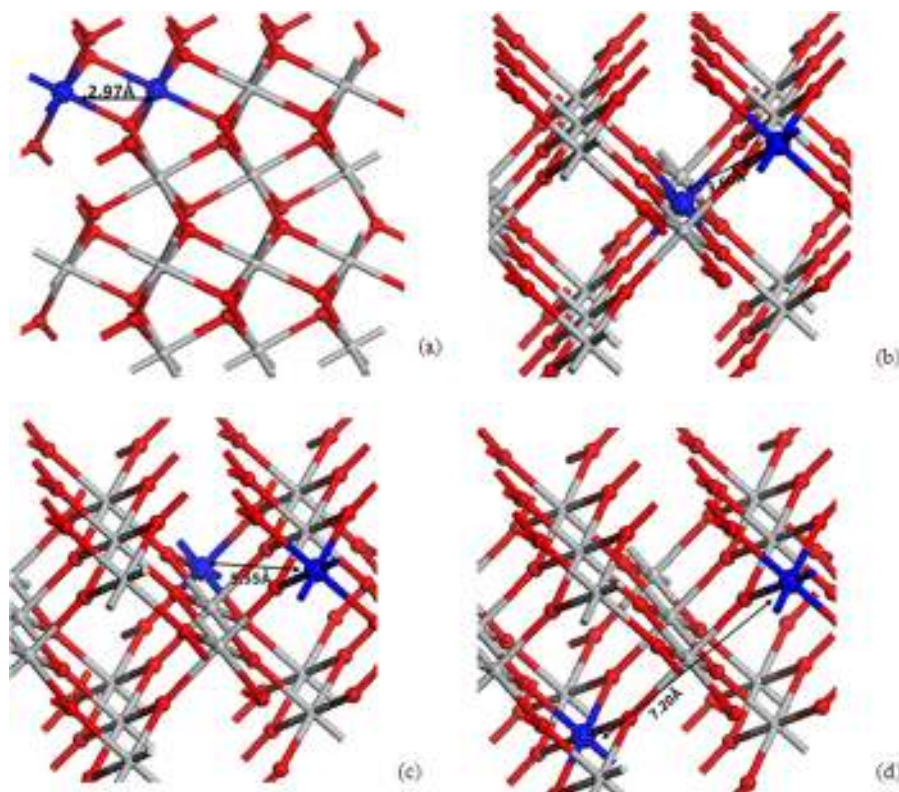

Figure 7. Doped TiO2 bulk with different dopant-dopant distances: (a) 2.97 Å, (b) 3.60 Å, (c) 5.54 Å, (d) 7.20 Å. The dopants are indicated with blue spheres.
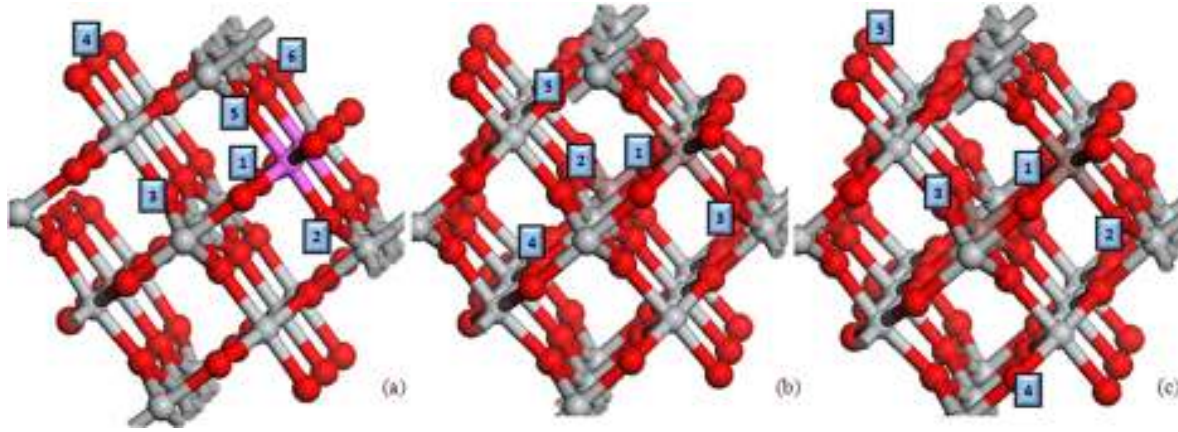
Figure 8. Oxygen vacancy positions for (a) Al, (b) Ga (with a Ga-Ga distance of 5.55 Å), (c) In.

From the structures with two dopants, we determine the most stable site for a compensating oxygen vacancy. For the oxygen vacancy calculations the Al-Al distance is 2.97 Å and the Ga-Ga distances are 2.97 Å and 5.55 Å, while the In-In distance is 3.60 Å. The oxygen vacancy sites are given in figure 8.

Table 3 presents the formation energies of the compensating oxygen vacancy in each doped structure from DFT+U. We find that the formation energies are generally very small and positive, with a number of dopant-vacancy configurations given negative formation energies. The latter configurations will therefore show spontaneous charge compensation via oxygen vacancy formation. Given that the present calculations are at 0K, the very low cost of forming the compensating oxygen vacancy in the other dopant-vacancy configurations means that under typical experimental conditions, dopant compensation through oxygen vacancy will occur. Thus, one would not expect to find a signature of an oxygen hole polaron defect state in experimental characterisation of trivalent doped TiO_2. For Al-doped TiO_2, experimental studies show that Al doping is compensated by oxygen vacancies [21, 22], while for Ga and In doping, the present results also indicate that charge compensation will occur. For each dopant, we have also computed the oxygen vacancy formation energy of the most stable vacancy compensated structure with HSE06, as a further check on the DFT+U findings. The formation energies are as follows: -0.85 eV (Al), -1.31 eV (Ga) and 1.21 eV (In). While hybrid DFT is more favourable towards oxygen vacancy compensation than DFT+U, the results of the DFT+U calculations are at least consistent with hybrid DFT, providing reasonable confidence in using DFT+U for these systems. However, when possible, a check on DFT+U results with hybrid DFT would be recommended for increased confidence.

O vacancy site	Al	Ga[a]	Ga[b]	In
	E^{Ovac}/eV			
OV1	0.27	0.05	-0.25	0.14
OV2	0.45	0.13	-0.27	0.32
OV3	0.75	0.38	0.22	0.12
OV4	0.75	0.18	-0.50	0.23
OV5	0.46	0.47	-0.50	- 0.31

Table 3. Formation energies (E^{Ovac} / eV) of compensating oxygen vacancies for Al, Ga and In doped TiO_2. All results are from the DFT+U method.

[a]: for a Ga-Ga distance of 5.55 Å, [b]: for a Ga-Ga distance of 2.97 Å

4. Conclusions

We have investigated doping of bulk TiO_2 with trivalent ions using standard DFT, DFT+U (with U on oxygen) and hybrid DFT (HSE06). We confirm that the DFT description of the oxygen hole is incorrect and find that both DFT+U and hybrid DFT give a solution with a localised oxygen hole and a distorted structure around the dopant site. The extent of distortion increases with an increase in the ionic radius of the dopant. The density of states shows a localised feature in the band gap characteristic of the oxygen hole. The DFT+U offset to the valence band is consistent with the hybrid DFT offset, but due to the band gap underestimation in DFT+U, the offset to the conduction band is too small. Oxygen vacancy compensation calculations show oxygen vacancy compensation of these dopants should occur.

References

1. Diebold U 2003 *Surf. Sci. Rep.* 48 53

2. Fujishima A, Zhang X and Tryk D A 2008 *Surf. Sci. Rep.* 63 515

3. Ni M, Leung M K H, Leung D Y C and Sumathy K 2007 *Renewable and Sustainable Energy Reviews* 11 401

4. Nowotny J 2008 *Energy Environ. Sci.* 2 565

5. Gurol M D Report "Photocatalytic construction materials and reduction in air pollutants" 2006 http://www.emeraldcoolpavements.com/pressrelease/SanDiegoStateEvaluation.pdf

6. Zhou Z G and Tang Z L 2009 *J. Inorg. Materials* 24 650

7. Yang J J, Pickett M D, Li X, Ohlberg D A A, Stewart D R and Williams R S 2008 *Nature Nanotechnology* 3 429

8 Cui Y, Du H and Wen L S 2008 *J. Mat. Sci. and Tech.* 24 675

9 Peng H W, Li J B, Li S S and Xia J B 2008 *J. Phys. Cond. Matt.* 20 125207

10 Nie X L, Zhou S P, Maeng G and Sohlberg K 2009 *Int. J. Photoenergy* 294042

11 Di Valentin C, Pacchioni G, Onishi H and Kudo A 2009 *Chem. Phys. Lett.* 469 166

12 Yu J G, Xiang Q J and Zhou M H 2009 *Appl. Cat. B Environmental* 90 595

13 Bian L, Song M X, Zhou T L, Zhao X Y and Dai Q Q, 2009 *J. Rare Earths* 27 461

14 Di Valentin C, Finazzi E, Pacchioni G, Selloni A, Livraghi S, Paganini M C and Giamello E 2007 *Chem. Phys.* 339 44

15. Czoska A M, Livraghi S Chiesa M, Giamello E, Agnoli S, Granozzi G, Finazzi E, Di Valentin C and Pacchioni G 2008 *J. Phys. Chem C* 112 8951

16 Long R and English N J 2010 *J. Phys. Chem. C* 114 11984

17 Zheng J W, Bhattcahrayya A, Wu P, Chen Z, Highfield J, Dong Z L and Xu R 2010 *J. Phys. Chem. C* 114 7063

18. Gai Y Q, Li J B, Li S S, Xia J B and Wei S H 2009 *Phys. Rev. Lett.* 102 036402

19 Zhu W G, Qiu X F, Iancu V, Chen X Q, Pan H, Wang W, Dimitrijevic N M, Rajh T, Meyer H M, Paranthaman M P, Stocks G M, Weitering H H, Gu B H, Eres G and Zhang Z Y, 2009, *Phys. Rev. Lett.* 103 2264101

20 Zhang J, Pan CX, Fang PF, Wie JH and Xiong R 2010 *ACS Applied Materials and Interfaces* 2 1173

21. Gesenhues D Solid 1997 *State Ionics, 101-103* 1171

22. Gesenhues U and Rentschler T 1999 *J. Solid State Chemistry* 143 210

23. Shirley R Kraft M and Inderwildi O R 2010 *Phys. Rev. B* 81 075111

24 Islam M M, Bredow T and Gerson A 2007 *Phys. Rev. B* 76 045217

25 Stashans A and Bermeo S 2009 *Chemical Physics* 363 100

26. Zwingel D 1978 *Solid State Communications* 26 775

27. Okajima T, Yamamoto T, Kunisu M, Yoshioka S, Tanaka Y and Umesaki N 2006 *Jap. Journal Applied Physics* 45 7028

28. Lee D-K and Yoo H-I 2008 *Phys Chem Chem Phys* 10 6890

29. Liu G A, Zhang J and He X M 2009 *Chin J. Inorg. Chem* 25 1939

30. Wang E, Yang W and Cao Y 2009 *J. Phys. Chem. C* 113 20912

31. Shchukin D, Poznyak S, Kulak A and Pichat P 2004 *J. Photochem and Photobiol A* 162 423

32. Gonzalez V R, Rodriguez A M, May M, Tzompantzi F and Gomez R 2004 *J. Photochem and Photobiol A* 193 266

33. Lany S, 2010 *Phys. Stat. Sol. B* doi: 10.1002/pssb.201046237

34. Lany S and Zunger A 2009 *Modelling and Simulation in Materials Science and Engineering* 17 084002

35. Morgan B J and Watson G W 2009 *Phys. Rev. B* 80 233102

36 Nolan M, Grigoleit S, Sayle D C, Parker S and Watson G W 2005 *Surf. Sci.* 576 1200

37 Fabris S, Vicario G, Balducci G, de Gironcoli S and Baroni S 2005 *J. Phys. Chem. B* 109 22860

38 Ganduglia-Pirovano M V, da Silva J L F and Sauer J 2009 *Phys. Rev. Lett.* 102 026101

39 Scanlon D O, Walsh A, Morgan B J and Watson G W 2008 *J. Phys. Chem. C* 112 9903

40 Nolan M, Elliott S D, Mulley J S, Bennett R A, Basham M and Mulheran P 2008 *Phys. Rev. B* 77 235424

41 Morgan B J and Watson G W 2007 *Surf. Sci.* 601 5034

42 Di Valentin C, Pacchioni G and Selloni A 2009 *J. Phys. Chem. C* 113 20543

43 Nolan M and Watson G W 2005 *Surf. Sci.* 586 25

44. Scanlon D O, Walsh A, Morgan B J, Nolan M, Fearon J and Watson G W 2007 *J. Phys. Chem. C* 111 7971

45 Nolan M and Watson G W 2006 *J. Chem. Phys* 125 144701

46 Han D, West D, Li X-B, Xie X-Y, Sun H-B and Zhang S B 2010 *Phys. Rev. B* 82 155132

47 Yeriskin I and Nolan M 2010 *J. Phys. Condens. Matt.* 22 135004

48 Anisimov V I, Zaanen J, and Andersen O K 1991 *Phys. Rev B* 44 943

49 Dudarev S L, Botton G A, Savrasov S Y, Humphreys C J, and Sutton A P 1998 *Phys. Rev. B* 57 1505

50 Huang P and Carter E A 2008 *Ann. Rev. Phys. Chem.* 59 261

51 Da Silva J L F, Ganduglia-Pirovano M V, Sauer J, Bayer V and Kresse G, 2007 *Phys. Rev. B* 75 045121

52 Deskins N A and Dupuis M 2007 *Phys Rev. B* 75 195212

53 Janesko B G, Henderson T M and Scuseria G E 2009 *Phys. Chem. Chem. Phys.* 11 443

54 Henderson T M, Paier J and Scuseria G E 2010 *Phys. Stat. Sol. B* doi:10.1002/pssb.201046303

55 Scanlon D O, Morgan B J, Watson G W and Walsh A 2009 *Phys. Rev. Lett.* 103 096405

56 Agoston P, Albe K, Nieminen R M and Puska M J, 2009 *Phys. Rev. Lett.* 103 245501

57 Marsman M, Paier J, Stroppa A and Kresse G, 2008 *J. Phys. Condens. Matt.* 20 064201

58 Nolan M 2010 *Chem. Phys. Lett.* 492 115

59. Nolan M 2010 *Chem. Phys. Lett.* 499 126

60. Kresse G and Hafner J 1994 *Phys. Rev. B* 49 14251; Kresse G and Furthmüller J 1996 *Comp. Mat. Sci* 6 5

61. Blöchl P E 1994 *Phys. Rev. B* 50 17953; Joubert D and Kresse G 1999 *Phys. Rev. B* 59 1758

62. Perdew J P, Burke K and Ernzerhof M 1996 *Phys. Rev. Lett.* 77 3865

63. Schirmer O F 2006 *J. Phys. Cond. Matt.* 18 R667

64 Stoneham A M, Gavartin J, Shluger A L, Kimmel A V, Munoz Ramo D, Ronnow H M, Aeppli G and Renner C 2007 *J. Phys. Cond. Matt.* 19 255208

65 Du M H and Zhang S B 2009 *Phys. Rev. B* 80 115217

66 Laegsgaard J and Stokbro K 2002 *Phys. Rev. B* 65 075208

67 Pacchioni G, Frigoli F, Ricci D and Weil J A 2001 *Phys. Rev. B* 63 054102

68. Kowalski P M, Camellone M F, Nair N N, Meyer B and Marx D, 2010 *Phys Rev Lett.* 105 146405

69. Ghijsen J, Tjeng L H, van Elp J, Eskes H, Westerink J, Sawatzky G A and Czyzyk M T 1988 *Phys. Rev. B* 38 11322; Elfimov I S, Yunoki S and Sawatzky G A 2002 *Phys. Rev. Lett.* 89 216403

70. Morgan B J and Watson G W, 2010 *J. Phys. Chem. C*, 114, 2321